Exploration of a horizontal confined impinging heated jet using both experimental and numerical methods

Mark Fahey[#], Sarah J Wakes* and Christopher T Shaw[+]
[#]Kahu Technologies, Mosgiel, New Zealand, mark.fahey@kahutech.com
*Department of Design Studies, University of Otago, PO Box 56, Dunedin, New Zealand, sarah.wakes@design.otago.ac.nz
[+]Topajka Shaw Consulting Ltd, 10 Kiwi Burn Place, RD 1 Te Anau, New Zealand, chris.shaw@ihug.co.nz

ABSTRACT

Impinging jets have been fascinating experimentalists and numerical modellers for many years with seemingly simple geometries revealing complex flow characteristics. Due to their high heat and mass transfer rates, impinging jets find wide use in engineering and industrial applications. Not only is the impinging jet interesting in isolation but it is often found as part of a more complex flow situation within an industrial setting. The dilemma for analysts under commercial pressure is always what level of detail is required for the results to be helpful but available in a reasonable time. The aims of this paper are:

- To understand a horizontal confined heated impinging jet using a combination of visualisation, experimental and numerical techniques.
- To understand the significance numerical modelling decisions can have in the context of an industrial setting.
- To make informed decisions about turbulence modelling dependent on the context of the flow problem.

1. INTRODUCTION

Numerical methods are increasingly being used to understand complex industrial flows. As computing resources are usually limited to some extent there is always a tension between how to model the flow successfully and maintaining a reasonable turnover time within the product development process. For analysts needing answers to progress the product design process within a tight industrial timeframe the question becomes, how much modelling is required and to what level of accuracy? This work uses such a simple geometry/complex flow problem to provide some insight into these questions. In essence, does the context of the modelling change the level of accuracy and detail of the fluid flow behaviour understanding required?

Impinging jets are flows that find a wide variety of use within an engineering and industrial context [1]. This is usually due to their high heat and mass transfer rates that leads to use in many heating, cooling and drying operations such as in the paper, electronics and textiles industries [2]. The mass transfer properties are exploited in applications such as mine ventilation, spray painting, rockets and vertical-take-off-and-landing vehicles [3]. As well as their many industrial and practical applications impinging jets lend themselves very well to being used as benchmark test cases for numerical validation as the relatively simple geometries have flow characteristics that can be extremely complex and challenging to model.

The current study considered a horizontal confined impinging jet onto a heated plate that delivers a mixture of forced and natural convection regimes depending on the velocity of the jet. This work is part of a larger project at an appliance manufacturer and was an essential study to understand some of the significant flow behaviours occurring in their products. A heated impinging jet is a situation that can occur, for example, in an oven where large thermal gradients drive natural convection and fan-driven flows lead to forced convection. It would be important in this context to understand the effect the jet has on the overall flow behaviour but not necessarily have pinpoint accuracy to obtain value from the results.

The aims of this paper therefore are:

- To understand a horizontal confined heated impinging jet using a combination of visualisation, experimental and numerical techniques.
- To understand the significance numerical modelling decisions can have in the context of an industrial setting.
- To make informed decisions about turbulence modelling dependent on the context of the flow problem.

2. BACKGROUND

2.1 IMPINGING JETS

The main characteristics of the flow behaviour of an impinging jet have been described [4] as nearly irrotational normal straining in the vicinity of the stagnation point; strong streamline curvature near the free edge; and in the flow parallel to the impingement surface, wall jet behaviour in which the zero of the shear stress does not coincide with the zero of the velocity gradient. Pressure reflections from the impingement surface dampen velocity fluctuations normal to the wall, causing both slower growth of the radial wall jet compared to a free-air jet and sensitivity of the flow to streamline curvature [3]. These features prove to be somewhat difficult to represent with existing turbulence models [5]. Previous numerical studies of impinging jets have concentrated on turbulence or code performance. Jambunathan [6] reviewed heat transfer data for circular impingement jets and found that the configuration can have a large effect on heat transfer rates. Differences in experimental conditions could then lead to seemingly contradictory conclusions. Recently slot jets have attracted more attention as they offer higher cooling effectiveness, greater uniformity and more controllability [7]. Again a jet maybe confined or unconfined [5, 8]. Non-vertical configurations add complexity through non-uniform heating and buoyancy effects [8].

Nishino et al. [9] found that the k-ε turbulence model tends to overestimate the turbulent kinetic energy in the stagnation region for a confined horizontal axisymmetric jet impinging on a heated surface, leading to an over-prediction of heat transfer in the stagnation region. Measurements reveal that there is negative production of turbulent kinetic energy in the vicinity of the wall. A comparison of the k-ε turbulence model and a second moment closure model was undertaken with velocity measurements obtained from the stagnation and wall jet regions, [10]. It indicated the superiority of the second moment closure model in reproducing the observed mean velocities and normal and shear stresses.

2.2 TURBULENCE MODELS

A key indicator of the length of time a simulation may take is how the turbulence is handled. The tendency is that the simpler the turbulence model the less accurate it will be in predicting the flow although there are usually time advantages. The tension between these two aspects constantly needs to be re-evaluated as it depends on the physical situation, the computing resources and timeline available and the value needed from the results.

As is well known the Reynolds Averaged Navier-Stokes (RANS) approach decomposes the flow variables into mean and fluctuating components; a time-averaging approach that needs the integration time to be relatively long compared to the maximum period of the assumed fluctuations [11]. The incompressible RANS momentum equation becomes

$$\frac{\partial \rho \bar{u}_i}{\partial t} + \frac{\partial \rho \overline{u_i u_j}}{\partial x_j} = -\frac{\partial p}{\partial x_i} + \frac{\partial}{\partial x_j}\left(\mu\left[\frac{\partial \bar{u}_i}{\partial x_j} + \frac{\partial \bar{u}_j}{\partial x_i}\right] - \rho \overline{u_i' u_j'}\right) + f_i \tag{1}$$

where the term $\overline{u_i' u_j'}$ is called the Reynolds stress tensor. In order to compute the mean properties of the flow various methods have been proposed to determine this tensor. Within these types of models only the time-mean quantities are directly computed and nearly all of the small scales are modelled. The information lost in the Reynolds decomposition cannot be replaced by modelling and precludes the possibility for resolving small-scale interactions between turbulence and other physical phenomena; the actual physics is smeared over time.

Despite its many shortcomings, the RANS approach is commonly used in commercial CFD codes for industrial simulations [12] and it has been validated over a wide range of problems and its deficiencies are well known. RANS is considered as the most practical turbulence model for industrial CFD problems with the computational resources of the present day [13].

Two-equation eddy viscosity turbulence models offer a good compromise between accuracy and computational effort [12]. In its most basic form, a two-equation turbulence model consists of a partial differential equation for turbulent kinetic energy, k, and one for another variable, with ε being the most common [14, 15]. Some of the limitations of the k-ε model include [16]:

- The turbulent kinetic energy is over-predicted in regions of flow impingement and reattachment, leading to poor prediction of the development of flow around leading edges and bluff bodies.
- Regions of re-circulation in swirling flows are under-estimated.
- Highly swirling flows are generally poorly predicted due to complex strain fields.
- Mixing is poorly predicted in flows with strong buoyancy effects.
- The spreading rates of wakes and round jets are predicted incorrectly.
- Laminar and transitional regions of flow cannot be modelled with the standard k-ε model.
- Turbulent flows in near-wall regions are not predicted well without special treatment.

An alternative two-equation turbulence model is the k-ω model, where the second variable is the frequency of the vorticity fluctuations, ω. The k-ω model does not require the complex non-linear damping functions for near-wall treatment [12]. The model though is very sensitive to the free stream value of ω. A possible solution to this sensitivity is to use the k-ε model equations in the body of the flow blended into the k-ω model in the near wall region. With a limiter to the equation for eddy viscosity and accounting for the transportation of shear stress this is termed the k-ω based Shear Stress Turbulence (SST) model [17, 18]. The SST model gives accurate predictions of the onset and the amount of flow separation under adverse pressure gradients. The SST model has limited success for situations such as the behaviour of the flow downstream of the separation line, the proper simulation of vortex flows and situations where laminar-turbulent transition takes place [19].

Unsteady Reynolds-Averaged Navier Stokes (URANS) has proved to be deficient [20] as the solutions typically do not display the correct spectrum of turbulent scales, even if the model has sufficient spatial and temporal resolution. This is the result of the overly dissipative character of standard URANS methods and prevents the formation of a turbulence cascade starting from the large URANS structures [21].

Ideally the Direct Numerical Simulation of the Navier-Stokes equations would be used to resolve the complex behaviour of turbulent fluid flows. As the computational effort is excessive for engineering problems of practical importance it is beyond the limitations of current technology [22]. The next best approach is to resolve what can be afforded and apply a statistical model to account for the unresolved small scales, known as Large Eddy Simulation (LES). The computational effort required to solve LES is conservatively estimated at $\sim Re^2$ [11] and in the last decade computing power has reached a level to allow its use for practical flow problems. LES is still though relatively computationally expensive for industrial flow problems. A more practical alternative was proposed by Spalart et al. [23], known as Detached Eddy Simulation (DES).

Detached Eddy Simulation is a hybrid technique for the prediction of turbulent flows at high Reynolds numbers. It combines the advantages of the classical RANS formulation with elements of LES into one model. It relies on the comparison of the turbulent length-scale computed from the turbulence model with the local grid spacing [21]. In regions where the turbulent length scale is smaller than the local grid spacing and cannot be resolved, the RANS model is used. Where the grid is sufficiently fine enough to allow resolution of the large-scale part of the LES formulation, the DES model blends seamlessly from RANS to LES. This typically results in RANS being employed economically inside attached and mildly separated boundary layers and LES to massively separated regions [12]. It has been found by Mentor et al. [19], that DES simulations based on the SST-DES formulation show a significant improvement of the solution compared to the SST-RANS model.

The k-ε turbulence model was therefore chosen to be trialed along with the SST to examine the differences. It was anticipated that there maybe unsteadiness in the flow and LES was deemed too computationally expensive so SST-DES was also trialed.

3. METHODOLOGY

The experimental set-up is shown in Figure 1 and 2. A regulated supply of compressed air was delivered through a TSI4040 flowmeter and through flow straighteners into a horizontal pipe. The pipe has a 20mm inner diameter and a length of 700mm. The downstream end of the flow straightener section was covered by 15m gauze with 10% open area to reduce the length scale of turbulent structures entering the pipe. The flow from the pipe impinged on an 80mm diameter, electrically heated plate, embedded in a 300mm diameter wooden wall. The distance from the pipe exit to the impingement surface was fixed at 20mm, giving a jet diameter to plate distance ratio of one. The flow was confined between the impingement wall and another Perspex sheet opposite at the level of the jet exit. After impinging on the facing wall the flow left the system through the circumferential boundary between the two plates. The experiments were conducted in a closed room of dimensions 4m × 3m × 2.7m.

To measure the fluctuating flow velocity at a number of points, a single normal hot-wire probe was held from above, facing the rising flow. The probe was fixed such that it could be translated in three orthogonal directions aligned with the axis of the jet. Flow visualisation was provided using a laser and the flow seeded with a water-based oil (smoke) vapour, injected at points of interest.

The temperature of the heated plate was maintained at a constant 80°C, which required adjustment of a variable transformer to balance heat lost to the impinging flow. Further

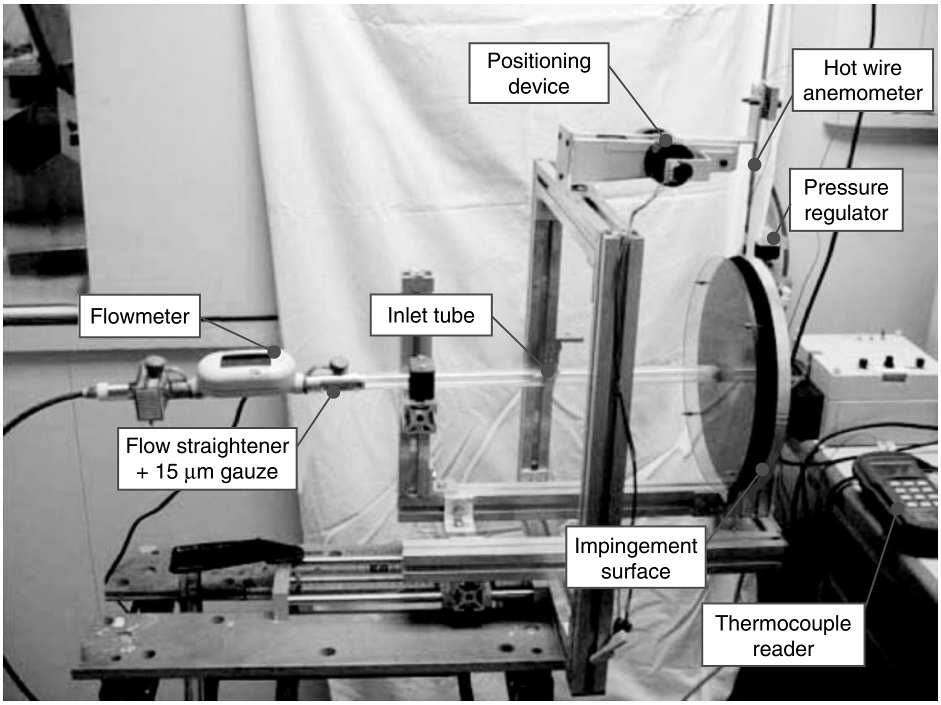

Figure 1 Impinging jet apparatus.

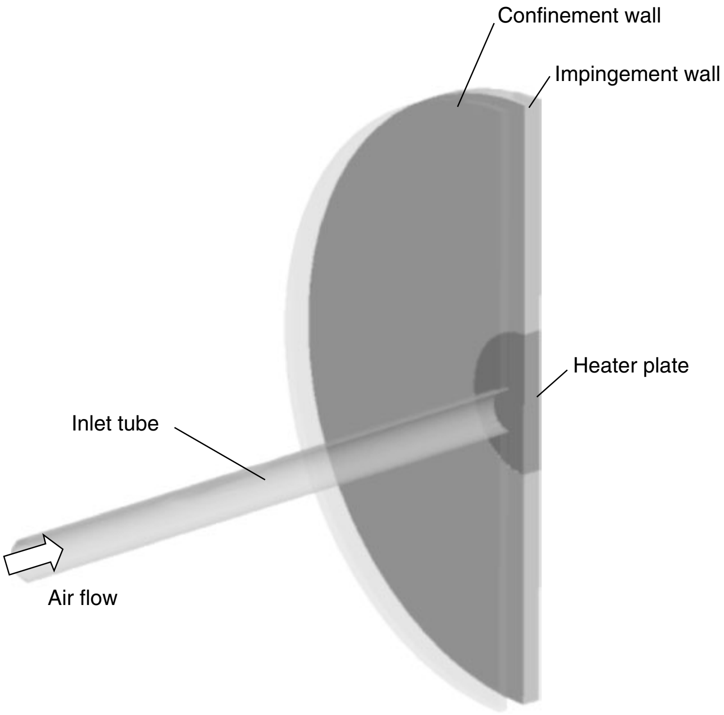

Figure 2 Schematic cross-section of impinging jet apparatus.

Table 1 Inlet velocities and Reynolds Numbers used in impinging jet experiment.

Case	Inlet Velocity [m/s]	Reynolds Number
1	0.00	0
2	0.20	274
3	0.50	685
4	1.00	1370
5	2.00	2740

Table 2 Impinging jet CFD cases.

Case	Inlet Velocity	Temperature	Mesh	Turbulence model
1	0.0m/s	80°C	800k	laminar
2a	0.2m/s	80°C	760k	k-ε
2b				SST
3a	0.5m/s	80°C	800k	k-ε
3b				SST
3c	0.5m/s	80°C	800k	Transient SST
3d	0.5m/s	80°C	800k	DES
4a	1.0m/s	80°C	800k	k-ε
4b				SST
5a	2.0m/s	80°C	800k	k-ε
5b				SST

temperature measurements were taken from the ambient air, the incoming flow and at the location of the hot-wire probe. The incoming air was measured at 20°C ± 1°C.

The inlet flow velocity was found using the volume flow rate, Q, and the area of the pipe, A, based on the pipe's inner diameter, giving the inlet velocity as

$$U = \frac{Q}{A} \tag{2}$$

with the nominated inlet velocity values and their associated Reynolds numbers in the pipe based on pipe diameter in Table 1. The selection of velocities was intended to cover the range of convective regimes, from purely natural convection in case 1 to a forced convection being dominant in case 5.

The CFD cases run are shown in Table 2. Without reviewing the experimental data it would be reasonable to expect cases 1-4 to be laminar and case 5 to be in transition from laminar to turbulent. Figure 3 shows that in reality only case 1 can be considered laminar after the flow exits the nozzle and enters the impingement region. For this reason a turbulence model is used in cases 2-5 despite the likelihood of laminar flow in the inlet tube.

In the CFD model, a uniform velocity boundary condition was applied to the pipe inlet. The heater plate was specified as a non-slip, isothermal wall with a temperature of 80°C. The outer circumferential region between the two walls was specified as an opening with a zero static pressure applied and flow direction left unspecified. The remaining walls were specified as non-slip adiabatic walls.

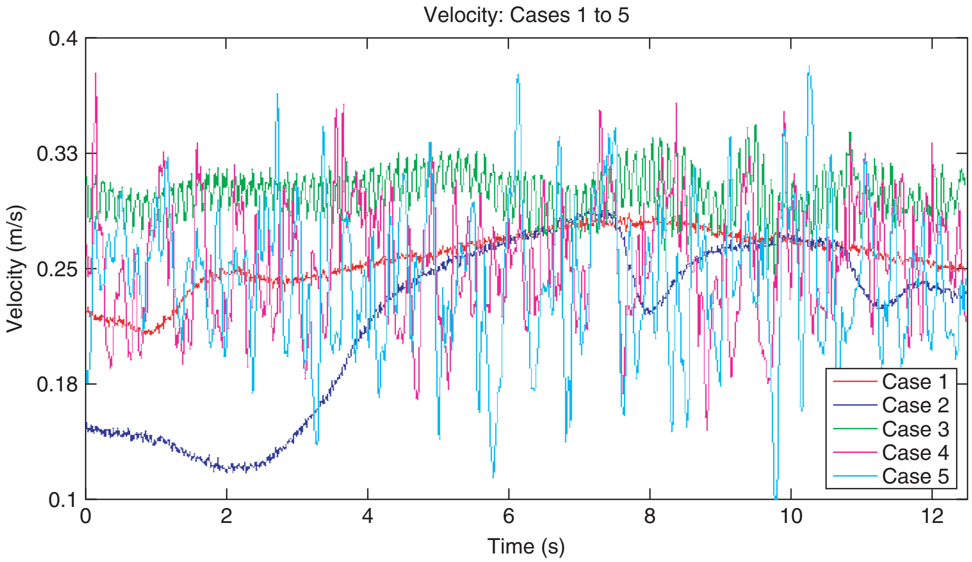

Figure 3 Sample of hot-wire velocities.

As the temperature differences within the fluid exceeded 10°C the Boussinesq buoyancy model was inappropriate. The fluid was therefore modelled as compressible to allow for variations in density and the full buoyancy model was used. The temperature of the inlet flow and the ambient temperature were taken as 20°C with the fluid being air as an ideal gas.

A zero-equation model was first run with all initial conditions set to zero with the turbulence model SST or k-ε reselected once the flow field was selected. The steady-state cases were run using the high resolution (near second-order) advection scheme. The use of transient SST and DES schemes were used to explore the unsteady behaviour observed in the flow.

The equations used within this problem are given in equations (3)–(6):

$$\frac{\partial \rho}{\partial t} + \frac{\partial \left(\rho u_i\right)}{\partial x_i} = 0 \tag{3}$$

$$\begin{aligned} \frac{\partial \left(\rho u_i\right)}{\partial t} + \frac{\partial \left(\rho u_i u_j\right)}{\partial x_j} = -\frac{\partial p}{\partial x_i} + \frac{\partial}{\partial x_j}\left(\mu\left[\frac{\partial u_i}{\partial x_j} + \frac{\partial u_j}{\partial x_i}\right]\right) \\ -\frac{\partial}{\partial x_i}\left(\frac{2}{3}\mu\delta_{ij}\frac{\partial u_k}{\partial x_k}\right) + f_i \end{aligned} \tag{4}$$

$$\frac{\partial \left(\rho c_v T\right)}{\partial t} + \frac{\partial \left(\rho u_i c_v T\right)}{\partial x_i} = \frac{\partial}{\partial x_i}\left(\frac{\partial}{\partial x_i} T\right) + q_T \tag{5}$$

with the buoyancy force term

$$f_{b_i} = \left(\rho - \rho_{ref}\right) g_i \tag{6}$$

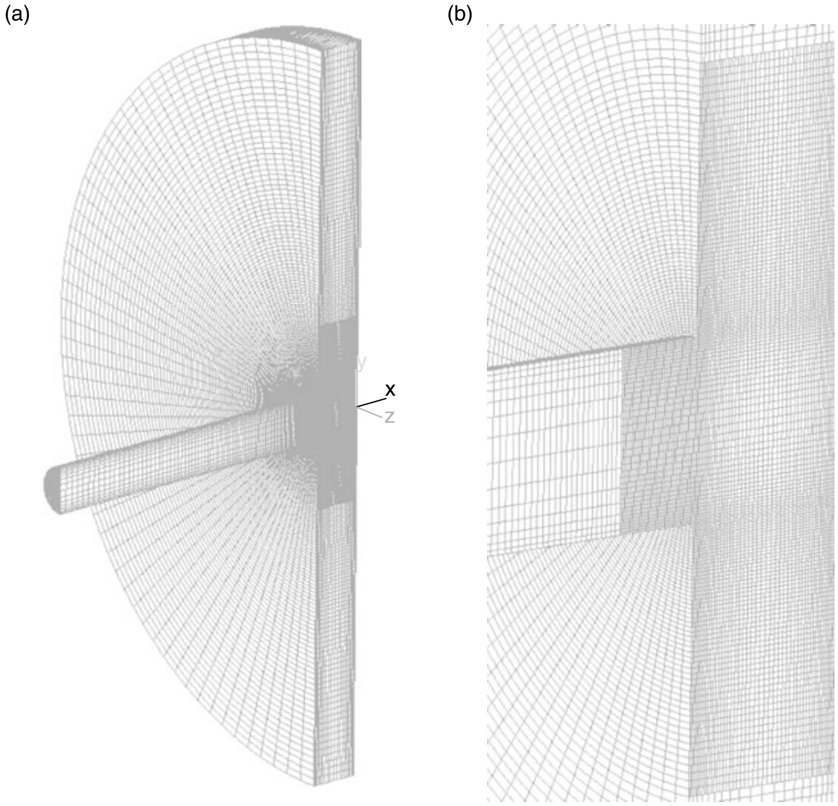

Figure 4 Mesh for impinging jet: (a) Fluid domain (b) Impingement region.

where u_i are the components of the mean velocity vector, ρ is the fluid density, t is time, p is the pressure, μ is the absolute viscosity, f_i is the external body force vector, δ_{ij} is Kronecker's delta. T is the temperature, c_v is the heat capacity at constant volume, k is the thermal conductivity of the fluid and q_T is the body heat source term. The commercial code used in this work, CFX, uses finite volume discritised formulation. The pressure and velocity are decoupled using a single cell, unstaggered, collocated grid to overcome *checkerboard* oscillation issues. Shape functions are used to evaluate the diffusion terms in the governing equations and the pressure gradient term. The advection term is discretised using an upwind formulation. The hydrodynamic equations for velocity and pressure are solved as a single system using a coupled solver that is fully implicit in time. Further details can be found in the CFX manual [12]. Figure 4 gives one half of a typical mesh used for the steady and URANS simulations.

4. RESULTS

In order to understand better the flow behaviour for each case the visualisation data is presented first followed by a comparison between the steady CFD and experimental data. Finally the transient CFD results are discussed. The flow visualisation provided non-quantitative but useful information on the flow behaviour within two distinct planes and aided the understanding of the other measurement results. The CFD results were being compared against both the flow visualisation and the hotwire data. A full picture of the flow

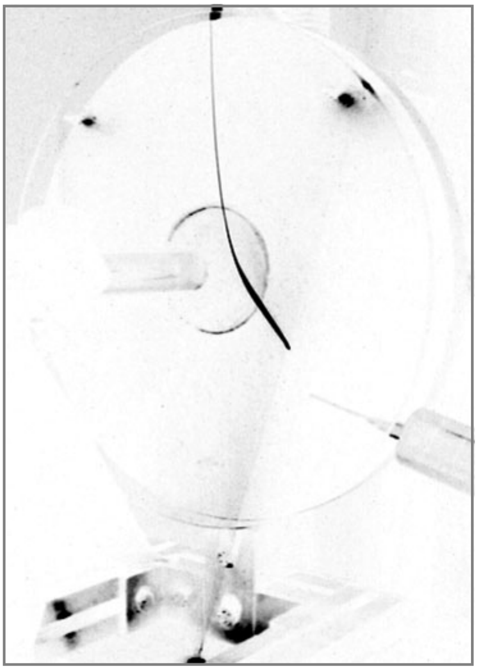

Figure 5 Case 1, normal plane.

can not be obtained without these three sets of results. In order to assess the effectiveness of each method overall flow predictions were compared as well as spot data with knowledge of the limitations of each of the methods. It was important to assess if the main features of the flow are being obtained and also how closely the spot data corresponds both in terms of trends and also accuracy.

4.1 FLOW VISUALISATION

Figures 5–9 show the flow visualisation for cases 1-5. Case 1 has no flow in the inlet pipe and hence no impinging jet as shown in figure 5. The injected smoke being entrained in the convecting air from the heater plate creates the streakline seen. Buoyancy effects lift the flow inwards and upwards through the space between the two plates. The low diffusion of the streakline indicates low levels of turbulence.

Figure 6 shows that in case 2 the turbulence levels are also relatively low. The interaction between the forced flow of the impinging jet and the buoyant flow. The underside of the impinging jet meets the heater plate surface and turns down. This then meets the buoyant air stream that results in the formation of a helical vortex near the impingement wall, with a second vortex rotating in the opposite direction approximately midway between the plates. The helical vortices spiralled to their left and right sides of the impingement region.

There is an increased level of turbulence shown in figure 7 for case 3 by the diffusion of the smoke. There is an obvious clear region in the centre of the heater plate where the clean air from the impinging jet exits the pipe. The injected smoke highlights the U-shaped helical vortex that wraps itself around the underside of the impingement region and rises on both

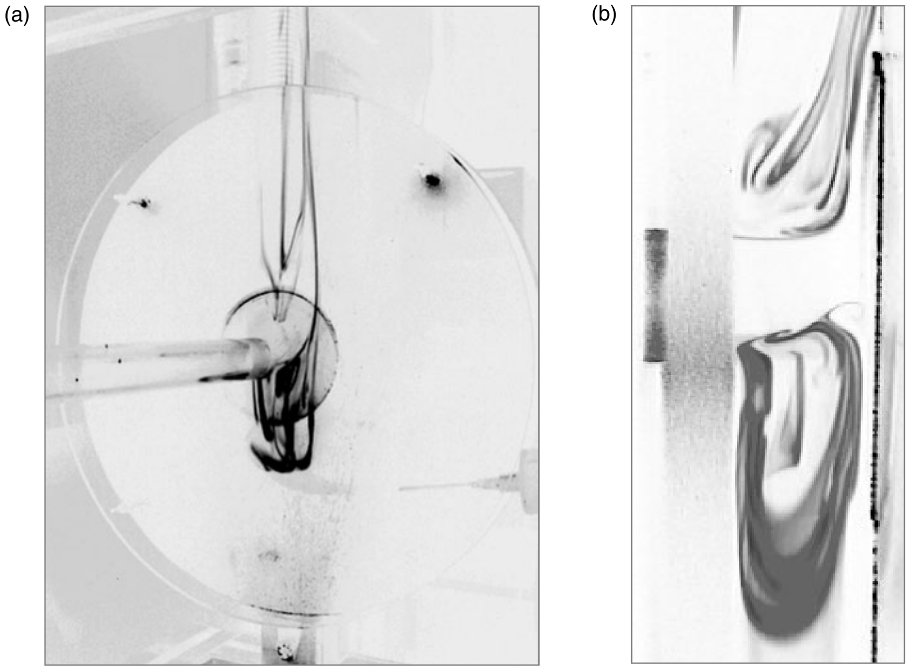

Figure 6 Case 2. (a) Normal plane. (b) Parallel plane.

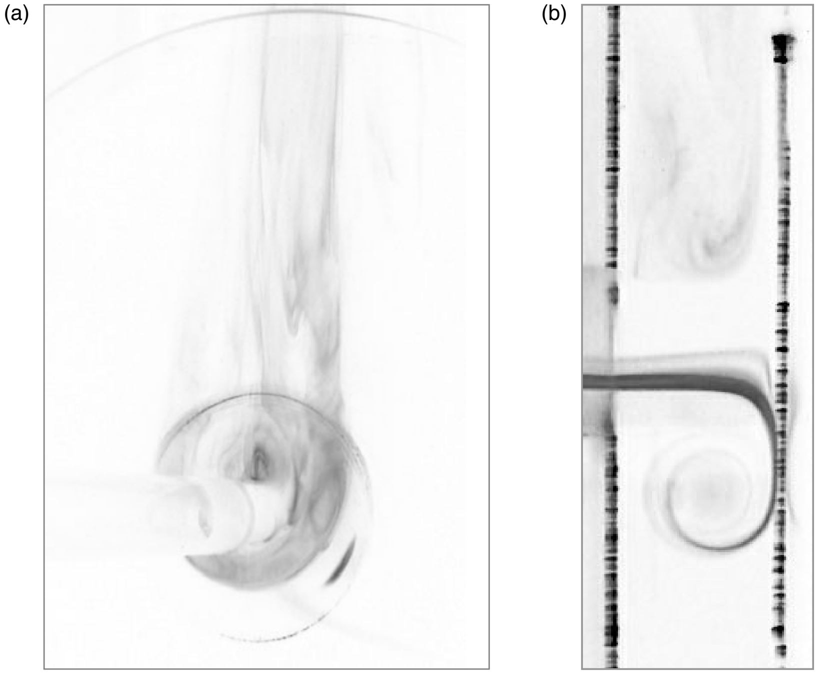

Figure 7 Case 3. (a) Normal plane. (b) Parallel plane.

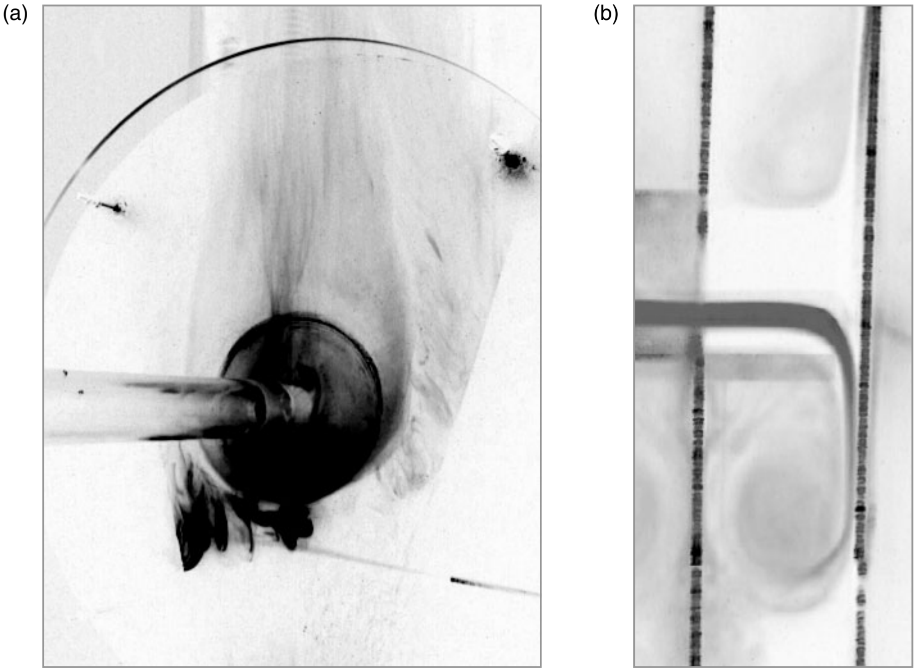

Figure 8 Case 4. (a) Normal plane. (b) Parallel plane.

sides. This single vortex can be seen to be significantly larger than the vortices in case 2. In this case the momentum of the jet is sufficient for it not to be bent upwards by buoyancy effects prior to impingement.

Case 4 showed similar flow patterns to case 3, figure 8, with a plume larger than the diameter of the heater plate. Mixing is occurring between the air delivered through the impinging jet and entrained air surrounding the impingement region. The momentum of the flow carries the impinging jet further down the wall than in previous cases before the effects of buoyancy turn the flow upwards.

Figure 9 shows that for case 5 with the highest inlet velocity studied, that the diameter of the impingement region is approximately twice that of the heater plate. The spread of the jet is also seen as it impinges on the heater plate. Buoyancy effects are still present in spite of the momentum of the jet.

4.2 EXPERIMENTAL AND STEADY-STATE CFD COMPARISON

When using experimental techniques such as hot-wire anemometer measurements the positioning of the probe has to be carefully thought out. The flow visualisation results indicated that an area to investigate in more detail would be one side of the horseshoe-shaped thermal plume. Figure 10 shows a schematic of the probe locations. The horizontal plane on which the measurements were taken is 130mm above the axis of the jet. The hotwire was calibrated and the accuracy was estimated at 5%. The velocity was sampled at a frequency of 10kHz for 12.5 seconds resulting in 125,000 values per location per case. Following the velocity measurement the temperature of the fluid was measured at the same location with a small thermocouple and the hot-wire measurements were corrected for the difference between the temperature during calibration and the temperature during measurement.

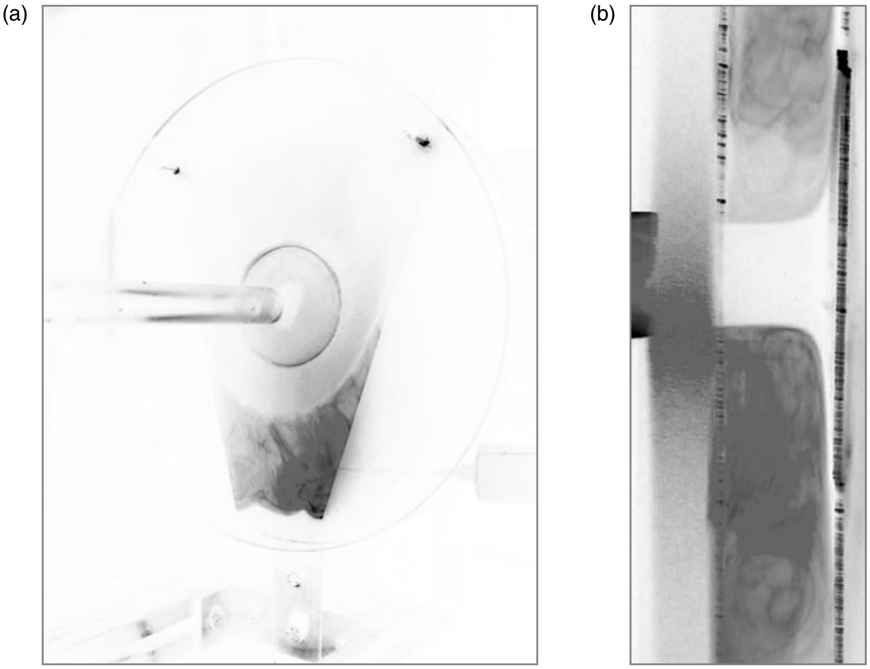

Figure 9 Case 5. (a) Normal plane. (b) Parallel plane.

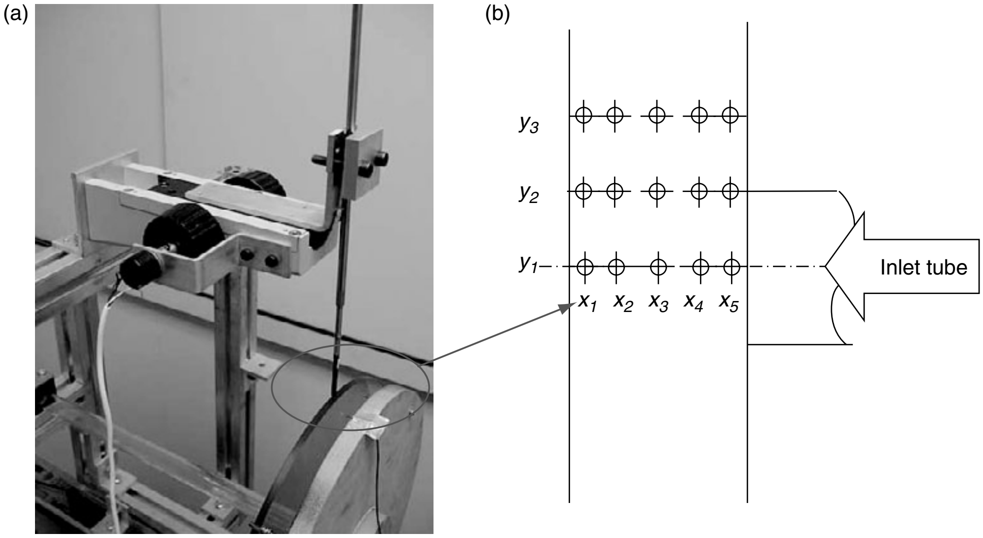

Figure 10 Hot-wire measurements. (a) Probe orientation. (b) Locations.

The first interesting observation from the hot-wire measurements is shown in figure 3. It can be seen looking at one point that as the velocity of the inlet flow increases as does the amplitude and frequency of the signal. For cases 4 and 5 the signal also appears random. The turbulence intensities are found at each of the 15 location and are shown in table 3 and

Table 3 Average turbulence intensity.

Case	Turbulence Intensity [%]
1	4.7
2	7.6
3	8.0
4	10.0
5	28.3

Table 4 Average integral time scales.

Case	Integral Time Scale [s]
1	1.48
2	1.06
3	0.78
4	0.21
5	0.15

confirm the increasing level of turbulence with increasing inlet velocity. It confirms that for cases 2-5 that a turbulence model is needed and that the turbulence intensity here is high and belies the small Reynolds Number in table 1. For cases 2-4 the k-ε turbulence model maybe appropriate but it is expected that for case 5 there will be scales of flow and transient behaviour that can only be captured with an unsteady simulation.

A calculation of the time integral scale is shown in table 4. This is calculated from the auto-correlation, R(τ) using equation 7.

$$R\left(\tau\right) = {}_{\tau}\underline{\lim}_{\bullet} \int_0^{\tau} u\left(t\right)u\left(t+\tau\right)dt \qquad (7)$$

The integral is calculated for every time-offset value, τ. The time-offset, τ, at which the normalised auto-correlation value reduces to zero is the time integral scale. This is an indication of the time period after which the signal becomes unrecognisable from its present state. With low levels of turbulence the hot-wire signal remains correlated with itself for relatively long periods. High levels of turbulence cause the correlation to diminish rapidly. It can be seen that the time scale decreases from case 1 to 5.

The hot-wire data highlights the unsteady nature of the flow. This leads to a question that is typical for most flows – what is the average velocity and how meaningful is it? It is likely that the sample times used here are not long enough to be sure of the long-term average.

Figures 11–15 show the comparison between the hot-wire anemometer data and the steady CFD results. The location (x_1, y_1) is plotted closest to the graph's origin and the five x positions are plotted according to their position across the 20mm distance between the two plates. The matrix contains ratios of the velocity predicted by CFD at each location to the average value of the hot-wire measurement at that location. Within the matrix the closer the value is to one the better the agreement between the CFD and hot-wire results.

Figure 11 shows that there is good agreement between the CFD results and the hot-wire data in the two rows near the impingement wall for case 1. In the final two rows the CFD velocities were significantly lower than the measured. Although the absolute values do not match well the overall trends are correctly predicted.

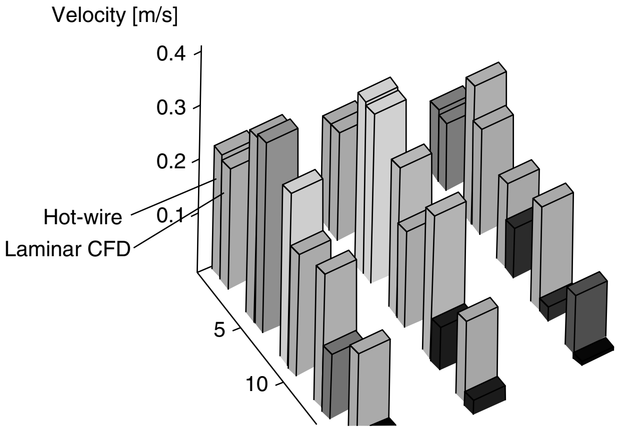

$$N = \begin{pmatrix} 1 & 1 & 1 \\ 1 & 1 & 0.8 \\ 0.7 & 0.6 & 0.6 \\ 0.5 & 0.3 & 0.1 \\ 0.2 & 0.2 & 0.1 \end{pmatrix}$$

Figure 11 Case 1 velocity comparison graph and normalised comparison matrix.

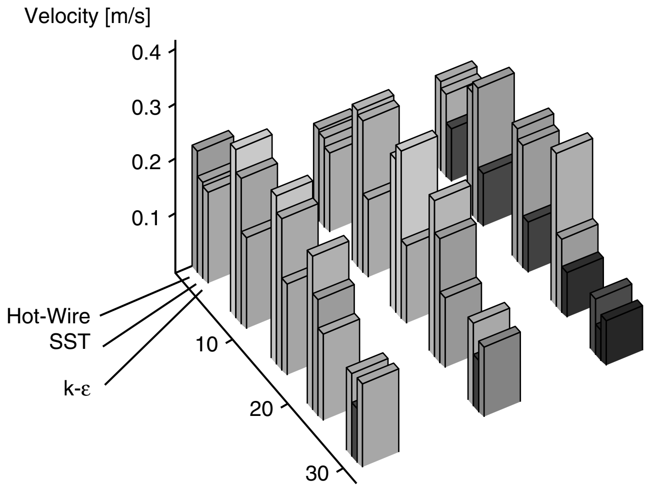

$$N_{SST} = \begin{pmatrix} 0.8 & 1 & 0.9 \\ 0.9 & 1 & 1.1 \\ 0.9 & 1.1 & 0.9 \\ 0.8 & 0.8 & 0.5 \\ 0.6 & 0.7 & 0.5 \end{pmatrix}$$

$$N_{K\varepsilon} = \begin{pmatrix} 0.8 & 0.9 & 0.6 \\ 0.6 & 0.5 & 0.4 \\ 0.6 & 0.5 & 0.4 \\ 0.6 & 0.5 & 0.3 \\ 1 & 0.9 & 0.8 \end{pmatrix}$$

Figure 12 Case 2 velocity comparison graph and normalised comparison matrices.

In cases 2–5 the relative performances of the k-ε and SST turbulence models with the hot-wire data are illustrated in figures 12–15. Figure 12 shows that the k-ε model under predicts at virtually all positions whereas the SST model compares much more favourably. In case 3, figure 13, the picture is very similar to that for case 2 although the SST model does over predict some values. For case 4, figure 14, the SST is mostly over predicting whilst the k-ε is doing both. Case 5, figure 15, with the highest turbulence intensity neither steady state turbulence model is doing a good job.

The literature has suggested that the k-ε model struggles to predict the complex flow situation created by the impinging jet case. The results confirm this position with the SST model performing better overall that the k-ε. There is definitely a case for performing an unsteady simulation from these results.

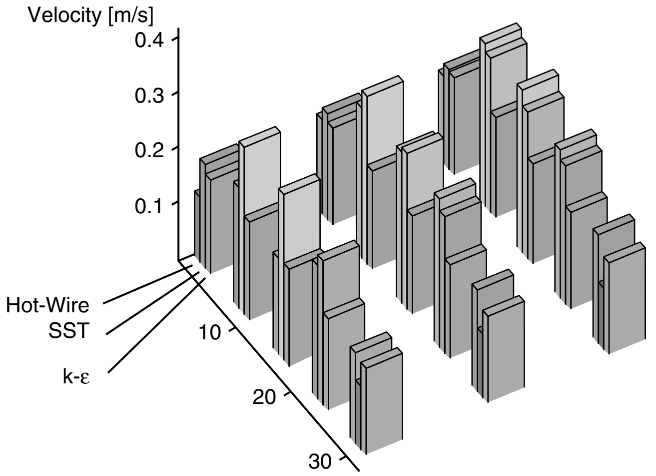

$$N_{SST} = \begin{pmatrix} 1.6 & 1.1 & 1.2 \\ 1.4 & 1.1 & 0.9 \\ 1.7 & 1 & 0.9 \\ 1.1 & 0.9 & 0.9 \\ 0.7 & 0.6 & 0.6 \end{pmatrix}$$

$$N_{K\varepsilon} = \begin{pmatrix} 1.5 & 1 & 1.2 \\ 0.8 & 0.7 & 0.6 \\ 1 & 0.7 & 0.6 \\ 0.7 & 0.6 & 0.7 \\ 1 & 0.9 & 0.9 \end{pmatrix}$$

Figure 13 Case 3 velocity comparison graph and normalised comparison matrices.

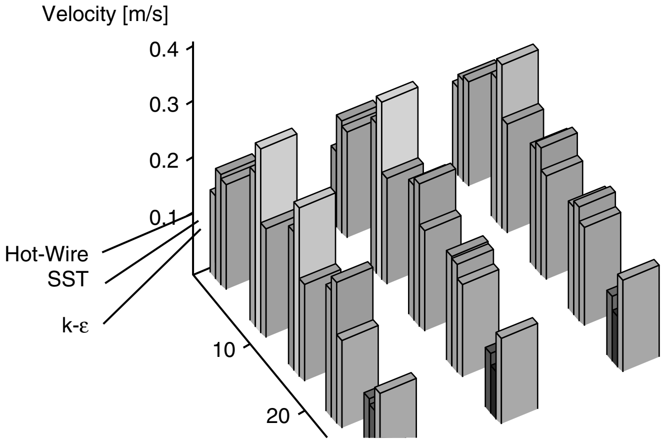

$$N_{SST} = \begin{pmatrix} 1.4 & 1.5 & 1.2 \\ 1.2 & 1.2 & 1.1 \\ 1.2 & 1.1 & 1.1 \\ 1.1 & 1 & 1.1 \\ 0.9 & 0.8 & 0.8 \end{pmatrix}$$

$$N_{K\varepsilon} = \begin{pmatrix} 1.3 & 1.4 & 1.2 \\ 0.7 & 0.7 & 0.8 \\ 0.7 & 0.8 & 0.9 \\ 0.7 & 0.9 & 0.9 \\ 1.3 & 1.5 & 1.4 \end{pmatrix}$$

Figure 14 Case 4 velocity comparison graph and normalised comparison matrices.

Figure 16 shows a flow visualisation for the two turbulence model flow fields for case 2 and the k-ε turbulence model performs poorly in comparison with the SST turbulence model. It can be seen that the k-ε model does not predict several of the vortices present and does not fully represent the interaction of the forced flow of the jet and the buoyant flow rising past the heated plate. Figure 17 shows that in comparison with the flow visualisation the SST results capture this interaction well. The pair of vortices is reproduced as is the radial spread of the impinging jet. Esch et al. [24] also reported that the k-ε model over predicts the turbulent kinetic energy in the stagnation region and does not correctly resolve the development of the boundary layer downstream.

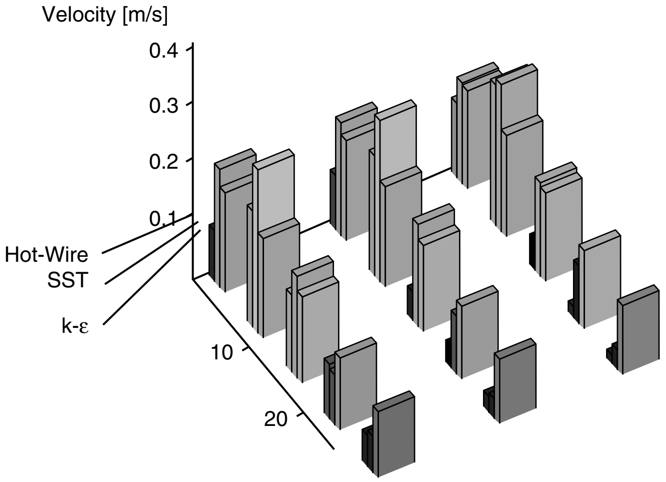

$$N_{SST} = \begin{pmatrix} 2.4 & 2.1 & 1.4 \\ 1.4 & 1.4 & 1.1 \\ 1.3 & 3.2 & 3.2 \\ 1 & 2.7 & 6.3 \\ 0.6 & 1.1 & 2.6 \end{pmatrix}$$

$$N_{K\varepsilon} = \begin{pmatrix} 2.1 & 1.9 & 1.4 \\ 0.9 & 0.9 & 0.8 \\ 1.1 & 2.8 & 3.1 \\ 1.3 & 3.5 & 8.8 \\ 2.4 & 4.1 & 8.9 \end{pmatrix}$$

Figure 15 Case 5 velocity comparison graph and normalised comparison matrices.

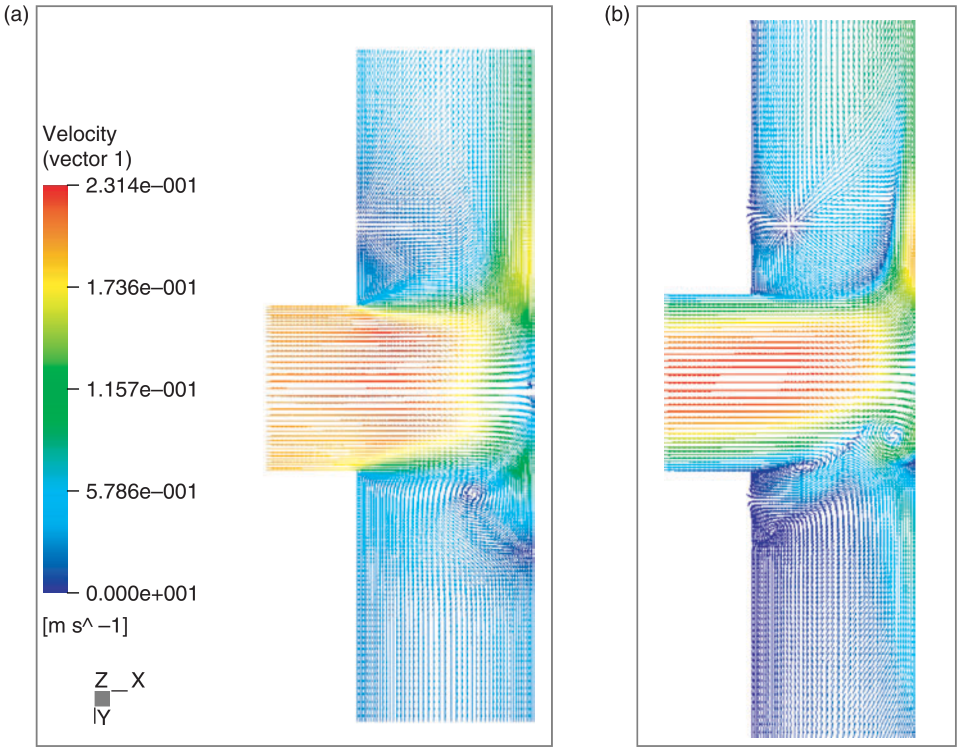

Figure 16 Case 2 steady-state CFD (a) k-ε (b) SST.

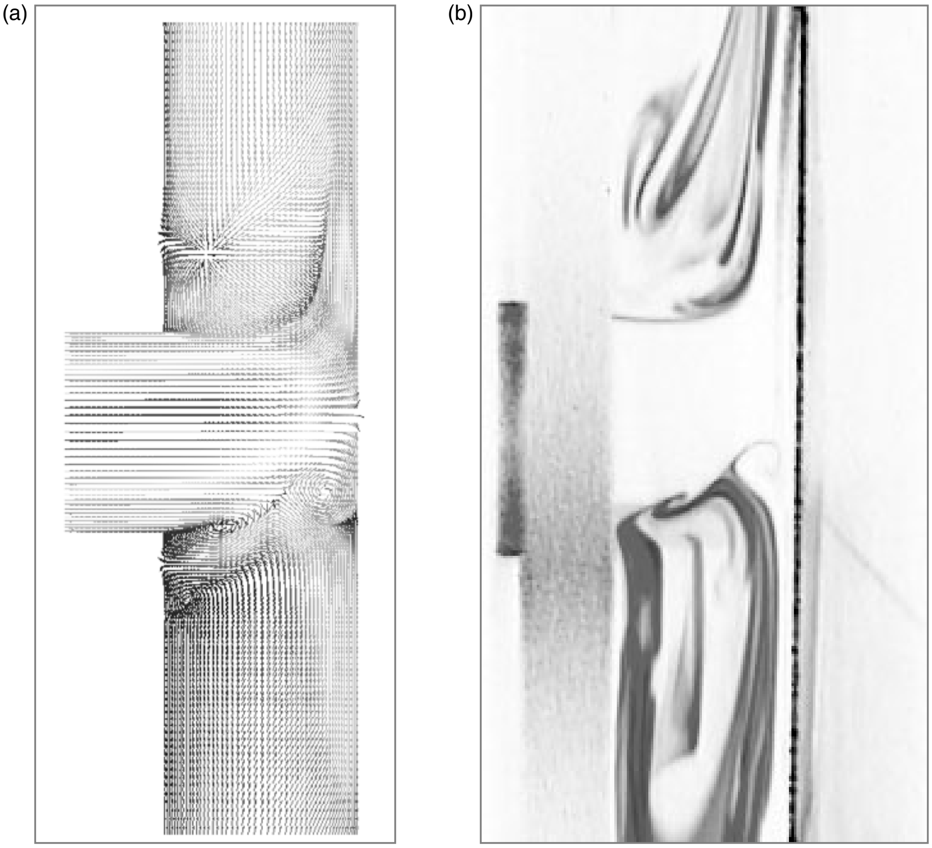

Figure 17 Case 2 steady-state CFD. (a) SST. (b) Flow visualisation.

It should be noted that the SST model does not match the flow visualisation in all cases. Figure 18 shows in case 3 that the size of the post-impingement flow region predicted by CFD is different in both shape and size to that shown in the flow visualisation. It can be seen that at the impact area at the plate the spread of the jet in the numerical simulation is too large and the plume too wide. There were also other issues with the convergence of the CFD steady-state model with the SST model. The k-ε model reaches convergence, damping out any tendency for the solution to detect transient behaviour, thought to be due to being overly dissipative. It is possible that the SST model was unable to reach convergence due to the unsteadiness of the solution as seen experimentally.

4.3 TRANSIENT CFD

Case 3 was chosen to be examined using transient CFD simulations using the same mesh as the steady simulation. The case was rerun firstly with the SST turbulence model and a time-step size of 0.01 seconds. The velocities were extracted at 0.1 second intervals and a total of 5.8 seconds was simulated. It took 11 hours of solution time per second of simulation. Figure 19 shows that although there was initial unsteadiness the transient behaviour lapsed back to steady-state values. Further insight is gained from examining the turbulent timescale. The average turbulent kinetic

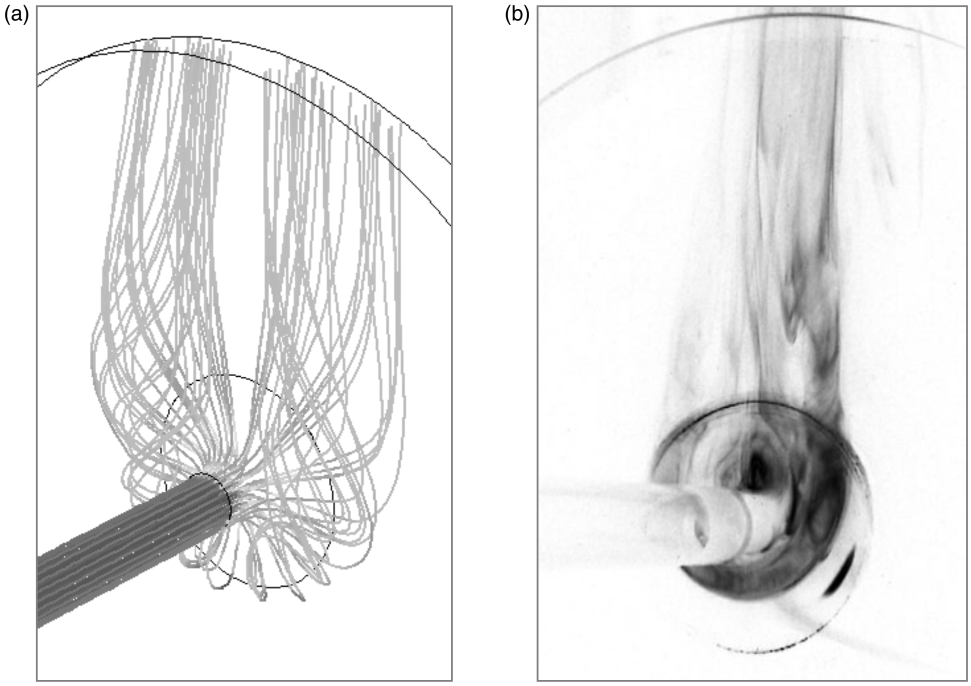

Figure 18 Case 3 steady-state CFD. (a) SST. (b) Flow visualisation.

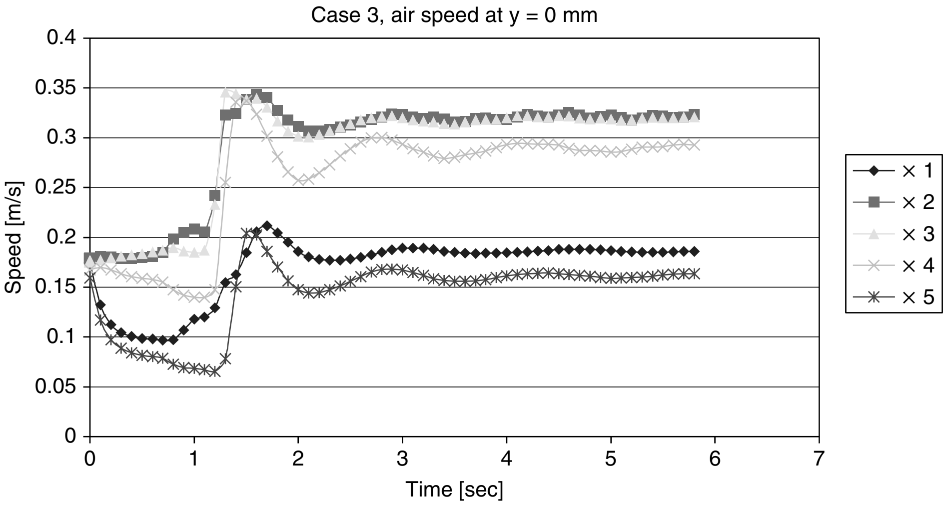

Figure 19 Case 3 URANS results.

energy, k, in case 3 is $0.00199\text{m}^2/\text{s}^2$ and the average turbulent eddy dissipation, ε, is $0.0121\text{m}^2/\text{s}^3$. An indication of the turbulence timescale is given by the ratio

$$\frac{k}{\varepsilon} = 0.164s \tag{8}$$

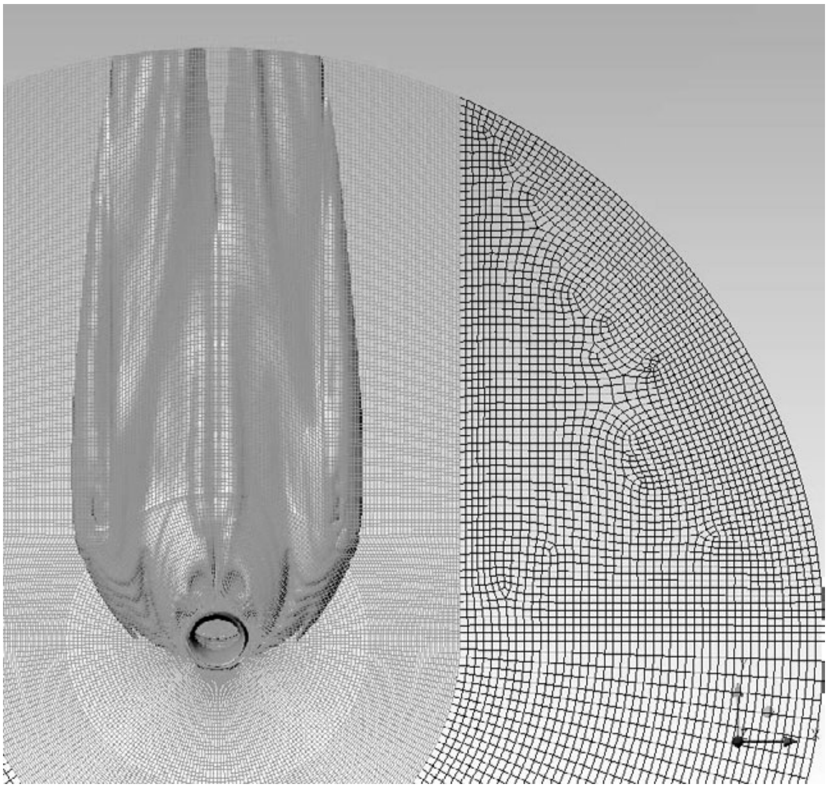

Figure 20 Iso-surface showing interface between RANS and LES.

For unsteady Reynolds Averaged Navier Stokes (URANS) simulations the turbulence timescale should be significantly less than the timescale of the gross flow oscillations. This ensures that the turbulence quantities are changing at a faster rate than the flow is changing. In case 3 the fluctuations are occurring at 9Hz, which gives a timescale of 0.11 seconds. Therefore the URANS approach is unable to resolve the turbulent scales of interest.

The failure of the URANS approach indicates that a more sophisticated and time-intensive turbulence approach is needed. DES was employed in this capacity; the computational expense is minimised by using RANS to model turbulence properties where the length-scale cannot be resolved. LES is used where the length-scale can be resolved. A finer mesh in the region of the impinging region was used and a total of 1.75 million elements were used as can be seen in figure 20. The DES solution was started with 0.0005 second time-steps and gradually increased to 0.005 second time-steps to produce 1.63 seconds of flow, taking several weeks using parallel processing, a considerably longer time than the URANS simulation.

Figure 20 shows an iso-surface marking the interface between the RANS (outside) and LES (inside) solutions. Figure 21 shows that two of the hotwire measurement locations lie within the LES region. The short amount of flow simulated limits the conclusions that can be drawn but as figure 22 shows the behaviour of the flow using DES is different from that of URANS. The frequency of fluctuations is 14Hz, within the ball park of the 9Hz found experimentally. Fluctuations were also found in other locations, including those computed

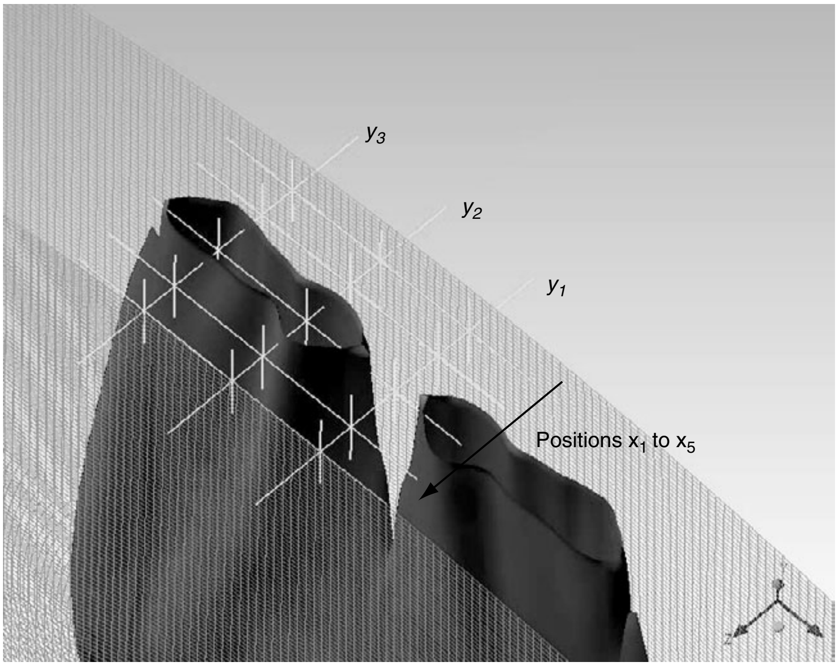

Figure 21 Measurement locations and Iso-surface between RANS and LES.

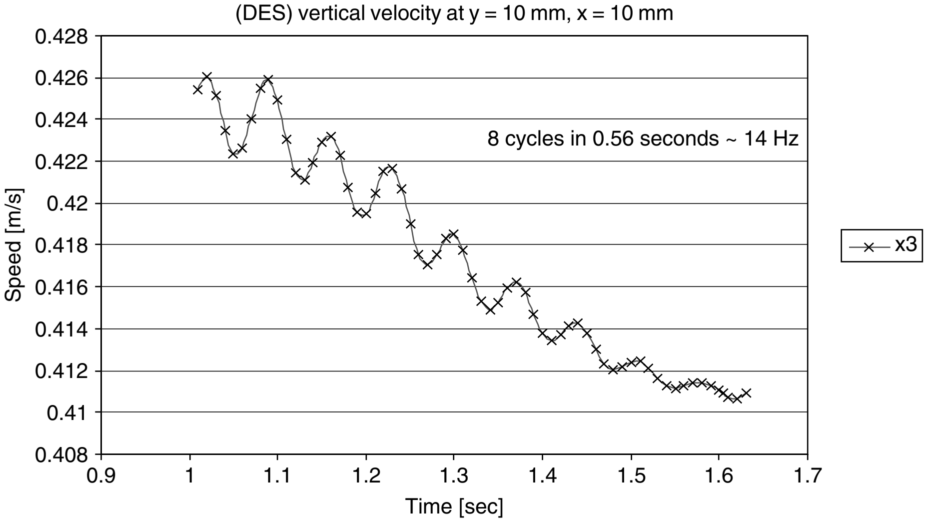

Figure 22 DES velocity data at location (x_3 , y_3).

with URANS. It seems likely that the LES is driving the fluctuations in the RANS region.

The velocity data is considerable higher than that of the hot-wire for the same location. It could be that the DES simulation is still in a transient phase where it is influenced by the dynamic response to the initial values. Also the short period of the simulation is not necessarily representative of the absolute values.

5. DISCUSSION

The impinging jet is an interesting case for experimental and numerical study. A simple geometry produces complex flow behaviour that proves to be difficult to reproduce using numerical techniques. This has implications for the use of CFD within an industrial setting. An impinging jet is not an unusual flow situation and this work has shown that it is unlikely that in the near future its simulation within real world problems will be possible with the accuracy that ideally we would wish. Even in this study with a simple geometry we were unable to model the flow to completion. It would be very unlikely to have months within an industrial setting to enable a DES study to be carried out. It highlights that compromises are often made when there are commercial pressures. All that can be done is recognise what will be modelled less accurately and weigh up the significance of such a compromise. This does not detract from the value of using CFD in such a complex multiphysics situation, just offers a note of caution.

Still valuable lessons from this simulation have been learnt. The SST turbulence model is far better than the k-ε in this situation, although it could not replicate the unsteady nature of the flow. For an impinging jet the use of the k-ε turbulence model may include loss of detail in the flow and damping of any natural unsteadiness in the flow. It did allow for flow calculations that are more likely to converge in a reasonable time and be stable. For the impinging jet the SST turbulence model was reasonably good at predicting the overall flow features but the unsteadiness proved to be very difficult and time consuming.

The impinging jet has a simple geometry but complex flow making it ideal for DES use. Use of LES within the DES model has the advantage of being a transient simulation and more of the scales within the turbulence are modelled. There is therefore more of a chance that the complexity of the impinging jet flow will be captured. Due to the finer mesh required and transient nature the major disadvantage is solution time to gain a meaningful period of simulation and it is often difficult to match a fluctuating flow. The combined use of visualisation, measurement and numerical modelling proved to be vital in establishing the complexity of the flow and the strengths of each method.

It is important for an analyst in an industrial situation to understand the limitations of the flows that are being modelled if only to make informed and rational decisions on the bounds of the complexity of the model to be used. It may, for example, only be necessary to explore such a situation intensively once as the insights can then be gained in multiple situations. The time it takes to get, if ever, a completely accurate model is potentially never going to be possible within an industrial timeframe. The bounds can therefore be established within which to work whilst still maintaining the integrity of the numerical model.

The analyst has to have an informed view as to what level of accuracy is right for the flow situation they are trying to emulate. In the impinging jet case for example if only the overall flow features were needed to predict heat transfer then the unsteadiness of the flow may not be an issue. Therefore a time-saving SST turbulence model would be sufficient and hence CFD could be used in a meaningful way within the product design process and not just to troubleshoot operational issues.

6. CONCLUSIONS

The following conclusions can be drawn from this work:

- The study highlighted the difficulty and effort required to achieve good agreement between CFD and experimental results. It was recognised that neither a numerical or experimental approach usually provides a perfect or complete representation of reality.

- The numerical and experimental approaches are complementary and when used appropriately they create a synergy that delivers greater benefit than either approach used in isolation.
- The flow in the impingement region of the jet was turbulent despite the Reynolds number of the flow in the inlet pipe indicating laminar flow.
- The buoyancy forces created in the flow by heat transfer from the heater plate interacted with the downward momentum of the flow on the underside of the jet and resulted in a prominent horse-shoe shaped vortex.
- The SST turbulence model proved more capable than the k-ε turbulence model of modelling the flow based on comparison between the CFD and hot-wire anemometry and flow visualisation.
- The experimental results detected a distinctive dominant frequency (unsteadiness) in the flow.
- URANS proved unsuccessful in replicating this due to the high turbulent viscosity suppressing the transient behaviour of the flow.
- The transient behaviour was captured using DES but further work is needed to confirm the effectiveness of this modelling approach.
- In the DES simulation the unsteadiness in the LES region propogated unsteadiness in the URANS region.
- Exploring a simple geometry/complex flow situation using both numerical and experimental approaches has provided insight into the assessment of the accuracy versus computational cost equation.
- It would have been difficult to fully understand the heated impinging jet without the three complementary techniques.

REFERENCES

1. Shuja, S.Z. and B.S. Yilbas, *A Laminar Swirling Jet Impingement on to an Adiabatic Wall.* International Journal of Numerical Methods for Heat and Fluid Flow, 2001. **11**(3): p. 237–254.
2. Park, T.S. and H.J. Sung, *Development of a Near-Wall Turbulence Model and Application to Jet Impingement Heat Transfer.* Int. J. Heat and Fluid Flow, 2001. **22**: p. 10–18.
3. Fairweather, M. and G.K. Hargrave, *Experimental Investigation of an Axisymmetric, Impinging Turbulent Jet. 1. Velocity Field.* Exp. Fluids, 2002. **33**: p. 464–471.
4. Craft, T.J., J.W. Graham, and B.E. Launder, *Impinging Jet Studies for Turbulence Model Assessment - II. An Examination of the Performance of Four Turbulence Models.* Int. J. Heat and Mass Transfer, 1993. **36**: p. 2685–2697.
5. Behnia, M., et al., *Numerical Study of Turbulent Heat Transfer in Confined and Unconfined Impinging Jets.* Int. J. Heat and Fluid Flow, 1999. **20**: p. 1–9.
6. Jambunathan, K., et al., *A Review of Heat Transfer Data for Single Circular Jet Impingement.* Int. J. Heat and Fluid Flow, 1992. **13**(2): p. 106–115.
7. Chen, Y.C., et al., *Theoretical Study of Impingement Heat Transfer with Single-Phase Free-Surface Slot Jets.* Int. J. Heat and Mass Transfer, 2005. **48**: p. 3381–3386.
8. Yan, X. and N. Saniei, *Heat transfer from an Obliquely Impinging Circular Air Jet to a Flat Plate.* Int. J. Heat and Fluid Flow, 1997. **18**: p. 591–599.
9. Nishino, K., et al., *Turbulence statistics in the Stagnation Region of an Axisymmetric Impinging Jet Flow.* Int. J. Heat and Fluid Flow, 1996. **17**: p. 192–201.
10. Dianat, M. and M. Fairweather, *Predictions of Axisymmetric and Two-Dimensional Impinging Turbulent Jet.* Int. J. Heat and Fluid Flow, 1996. **17**: p. 530–538.
11. McDonough, J.M., *Introductory Lectures on Turbulence*. 2004, Department of Mechanical Engineering and Mathematics, University of Kentucky.

12. ANSYS Inc, *CFX-5.7.1 Theory Manual*. 2005: ANSYS.
13. Subrata, R., K. Sagar, and J. Heidmann. *Film Cooling Analysis Using DES Turbulence Model*. in *ASME Turbo Expo*. 2003. Atlanta, Georgia, USA.
14. Dhinsa, K.K., C.J. Bailey, and K.A. Pericleous. *Turbulence Modelling and its Impact on CFD Predictions for Cooling of Electronic Components*. in *Inter Society Conference on Thermal Phenomena*. 2004.
15. Lai, J.C.S. and C.Y. Yang, *Numerical Simulation of Turbulence Suppression: Comparisons of the Performance of Four k-e Turbulence Models.* Int. J. Heat and Fluid Flow, 1997. **18**: p. 575–584.
16. WS Atkins Consultants, *Best Practice Guidelines for Marine Applications of Computational Fluid Dynamics*. 2002, MARNET-CFD Thematic Network: Epsom, U.K.
17. Menter, F.R. *Multiscale Models for Turbulent Flows*. in *24th Fluid Dynamics Conference*. 1993. Orlando, FL, U.S.A.
18. Menter, F.R., *A Comparison of Some Recent Eddy-Viscosity Turbulence Models. Journal of Fluids Engineering*, 1996. **118**: p. 514–519.
19. Menter, F.R. and M. Kuntz, *Development and Application of a Zonal DES Turbulence Model for CFX-5*. 2003, CFX-Validation Report, CFX-VAL 17/0503.
20. Kapadia, S. and S. Roy. *Detached Eddy Simulation Over a Reference Ahmed Car Model*. in *41st Aerospace Sciences Meeting and Exhibit*. 2003. Reno, NV, U.S.A.
21. Menter, F.R. and Y. Egorov, *A Scale-Adaptive Simulation Model using Two-Equation Models*, in *AIAA 2005-1095*. 2005, AIAA.
22. Speziale, C.G., *Turbulence Modeling in Non-inertial Frames of Reference.* Theor. Comput. Fluid Dyn., 1989. **1**(1) p. 3-19.
23. Spalart, P.R., et al., *Comments on the Feasibility of LES for Wings and on a Hybrid RANS/LES Approach*, in *Advances in DNS/LES*, C. Liu and Z. Liu, Editors. 1997, Greyden: Columbus, OH, U.S.A. p. 137–148.
24. Esch, T., F. Menter, and W. Vieser. *Heat Transfer Predictions based on Two-Equation Turbulence Models*. in *6th ASME-JSME Thermal Engineering Joint Conference*. 2003. Hawaii.

ACKNOWLEDGEMENTS

The authors gratefully acknowledge the assistance of Fisher & Paykel Appliance Ltd. and the Foundation for Science Research and Technology, Contract Number FSPX0001.